AGU PUBLICATIONS

Geophysical Research Letters

RESEARCH LETTER

10.1002/2016GL069873

Key Points:
- Brittle fragmentation theory is extended to represent emitted soil aggregates that are otherwise removed during soil characterization
- We reproduce the dust concentration and the nearly size-invariant fractional abundance of Fe off the coast of West Africa
- By distinguishing structural and free forms of elemental Fe model improvement can be attributed to emission of soil aggregates

Supporting Information:
- Supporting Information S1

Correspondence to:
C. Pérez García-Pando,
carlos.perezga@nasa.gov

Citation:
Pérez García-Pando, C., R. L. Miller, J. P. Perlwitz, S. Rodríguez, and J. M. Prospero (2016), Predicting the mineral composition of dust aerosols: Insights from elemental composition measured at the Izaña Observatory, *Geophys. Res. Lett.*, *43*, 10,520–10,529, doi:10.1002/2016GL069873.

Received 5 JUN 2016
Accepted 9 AUG 2016
Accepted article online 10 AUG 2016
Published online 13 OCT 2016

Predicting the mineral composition of dust aerosols: Insights from elemental composition measured at the Izaña Observatory

Carlos Pérez García-Pando[1,2], Ron L. Miller[1,2], Jan P. Perlwitz[1,2,3], Sergio Rodríguez[4], and Joseph M. Prospero[5]

[1]Department of Applied Physics and Applied Mathematics, Columbia University, New York, New York, USA, [2]NASA Goddard Institute for Space Studies, New York, New York, USA, [3]Now at Climate, Aerosol, and Pollution Research, LLC, New York, New York, USA, [4]Izaña Atmospheric Research Centre, AEMET, Joint Research Unit to CSIC "Studies on Atmospheric Pollution", Santa Cruz de Tenerife, Spain, [5]Rosenstiel School of Marine and Atmospheric Science, University of Miami, Miami, Florida, USA

Abstract Regional variations of dust mineral composition are fundamental to climate impacts but generally neglected in climate models. A challenge for models is that atlases of soil composition are derived from measurements following wet sieving, which destroys the aggregates potentially emitted from the soil. Aggregates are crucial to simulating the observed size distribution of emitted soil particles. We use an extension of brittle fragmentation theory in a global dust model to account for these aggregates. Our method reproduces the size-resolved dust concentration along with the approximately size-invariant fractional abundance of elements like Fe and Al in the decade-long aerosol record from the Izaña Observatory, off the coast of West Africa. By distinguishing between Fe in structural and free forms, we can attribute improved model behavior to aggregation of Fe and Al-rich clay particles. We also demonstrate the importance of size-resolved measurements along with elemental composition analysis to constrain models.

1. Introduction

Mineral dust created by wind erosion of soil particles in arid regions is one of the dominant aerosols by mass in the atmosphere, significantly affecting radiative fluxes [e.g., *Pérez et al*., 2006; *Miller et al*., 2014a], cloud properties [e.g., *DeMott et al*., 2003; *Seifert et al*., 2010], atmospheric chemistry [e.g., *Bauer and Koch*, 2005; *Chen et al*., 2011], ocean biogeochemistry [e.g., *Jickells et al*., 2005], and human health [e.g., *Pérez García-Pando et al*., 2014]. Models of mineral dust aerosols generally assume a globally uniform mineral composition. This simplification limits our understanding of the role of dust in the Earth system, since the climate effects of dust strongly depend on the particle physical and chemical properties that vary regionally with mineral composition.

Simulating the composition of dust aerosols in terms of their constituent minerals is challenging. Atlases of soil mineral composition [*Claquin et al*., 1999; *Nickovic et al*., 2012; *Journet et al*., 2014] are based upon measurements following wet sieving, a technique that breaks the aggregates found in the undisturbed parent soil [*Shao*, 2001]. During wind erosion, these soil aggregates are only partially fragmented by saltation and sandblasting on the soil bed, resulting in differences in the size distribution and composition of the wet-sieved soil and the particles that are potentially emitted. These differences have been generally neglected in previous models of aerosol mineral composition, leading to disagreements with respect to measurements of the emitted size distribution.

Recently, we proposed a method to calculate the emitted size distribution and mineral composition of dust aerosols that accounts for soil aggregates that are potentially emitted from the original undisturbed soil but are destroyed during wet sieving [*Perlwitz et al*., 2015a]. The method constructs the emitted size distribution of individual minerals building upon brittle fragmentation theory [*Kok*, 2011] and characteristic mineral size distributions estimated from observations [*Kandler et al*., 2009]. In *Perlwitz et al*. [2015b], we compared a global simulation incorporating this new approach to a baseline simulation in which the emitted mineral fractions were assumed to match those of the soil after wet sieving. An evaluation with a global compilation of mineral fraction measurements showed that, in contrast to the baseline, the new method reproduces the observed abundance of clay minerals (such as illite) at silt sizes, while reducing systematic overestimation of

quartz. The compilation of measurements presented in *Perlwitz et al*. [2015b] is derived from over 60 citations in the literature, but these typically come from field campaigns and ship cruises that are sporadic in space and time. In contrast, measurements at the Izaña Observatory, in the Canary Islands, provide a decadal record of size-resolved dust concentration and elemental composition. Dust reaching this site, and more generally the subtropical North Atlantic, arrives within the Saharan Air Layer (SAL) and is associated with the northeasterly trade winds blowing from North Africa [*Alonso-Pérez et al*., 2011, 2012; *Rodríguez et al*., 2015].

This contribution provides evidence from the long-term record at Izaña for the robust improvement of our emission model. In section 2, we describe the measurements at the Izaña Observatory and the essential aspects of the model, whose details are provided in *Perlwitz et al*. [2015a]. In section 3, we discuss the effect of soil aggregates upon the size distribution and elemental composition of dust measured at Izaña and downwind across the Atlantic. Conclusions are provided in section 4.

2. Data and Methods

2.1. Measurements

We compared our model with dust elemental composition measured at several size ranges measured at Izaña Observatory from 2002 to 2010 [*Rodríguez et al*., 2015]. Izaña is located in Tenerife Island (16°29′58″W; 28°18′32″N) at ~2400 m asl, which is well above the marine stratocumulus layer characteristic of the top of the subtropical marine boundary layer. In winter, dust concentration at Izaña is low as the Intertropical Convergence Zone (ITCZ) is at its southernmost position, and dust transport toward Tenerife is confined to the marine boundary layer [*Alonso-Pérez et al*., 2011]. In spring, short but intense dust events reach Izaña triggered by cold fronts penetrating into the northern Sahara [*Slingo et al*., 2006; *Knippertz and Todd*, 2012]. In summer, the ITCZ progresses northward, prompting intense easterly winds and the formation of the dusty SAL [*Prospero and Carlson*, 1972] over the Atlantic at altitudes between 1 and 5 km [*Tsamalis et al*., 2013], resulting in persistent dust at Izaña. The monitoring program, which is detailed elsewhere [e.g., *Rodríguez et al*., 2011, 2015] and described in the supporting information Text S1, includes the sampling (on microquartz filter at 30 m^3/h) and chemical characterization of total particulate matter (PM_T) and particulate matter with aerodynamic diameters smaller than 10 μm (PM_{10}) and 2.5 μm ($PM_{2.5}$). Each filter is bulk acidic digested, and the solution obtained is analyzed for the determination of the concentrations of major and trace elements by means of Inductively Coupled Plasma Atomic Emission Spectrometry. Errors are estimated to be ≤10%. Dust concentration is determined from the empirically derived sum $Al_2O_3 + SiO_2 + Fe + CaCO_3 + K + Na + Mg + P + Ti + Sr$ in the different size ranges. Si was derived indirectly from Al based on prior experiments ($SiO_2 = 3Al_2O_3$ [*Querol et al*., 2001]). Dust concentration was normalized so that when averaged over all bulk samples, Al accounts for 8% of the dust mass. This normalization is commonly applied in long-term dust records [*Prospero*, 1999; *Rodríguez et al*., 2012] and is also supported by the observed ratio of Al to PM mass determined by gravimetry of dust samples at Izaña (see supporting information Text S2 and Figures S1 and S2). Calcite—dissolved during acidification—was calculated from the amount of Ca not present as Ca sulfate and Ca nitrate. We note that the marine contribution to Na is negligible at Izaña [*Rodríguez et al*., 2011].

In section 3 we compare the model and observed monthly climatology (2002–2010) of dust concentration and the percent abundance of Si, Al, Fe, Mg, and Ca. The comparison is for total dust and three diameter (D) ranges: $D \leq 2.5$ μm (fine), $2.5 < D \leq 10$ μm (coarse), and $D > 10$ μm (supercoarse). Details on the generation of the monthly climatology from the individual samples are provided in the supporting information Text S1. We also compare the dust concentration calculated by the model to observations at Barbados (Ragged Point, 13.165°N, 59.432°W) between 2002 and 2010 [*Prospero and Lamb*, 2003; *Prospero and Mayol-Bracero*, 2013] and dust size distribution measured at Barbados from 5 April to 3 May 1994 [*Li-Jones and Prospero*, 1998]. A brief description can be found in the supporting information Text S3.

2.2. Modeling

We compare two methods to calculate the fractional size-resolved emission of minerals using the Coupled Model Intercomparison Project Phase 5 version of the NASA Goddard Institute for Space Studies Earth System ModelE [*Schmidt et al*., 2014; *Miller et al*., 2014b]. A detailed description of the dust module can be

found in *Miller et al*. [2006] and is summarized in the supporting information Text S4. The simulations were performed with a horizontal resolution of 2° latitude by 2.5° longitude and 40 vertical layers up to 0.1 hPa. The model circulation at each level was relaxed toward National Centers for Environmental Prediction reanalysis winds (using temporal interpolation in between the times corresponding to the four daily values), during the period of measurement at Izaña (2002–2010). Sea surface temperature and sea ice were prescribed from measurements [*Rayner et al*., 2003].

2.2.1. From Soil Mineral Fractions to Emitted Mineral Fractions

We provide a short description of the two approaches to calculate the size-resolved emission of each mineral. We refer to *Perlwitz et al*. [2015a] for a fuller description.

The Mean Mineralogical Table (MMT) by *Claquin et al*. [1999] provides the soil fractions of eight major mineral types in both the clay-size range (with diameters up to 2 μm) and the silt-size range (with diameters between 2 and 50 μm) as a function of arid soil type. The MMT derives from measurements based on wet sieving, a process that disturbs the soil samples, breaking the aggregates that are found in the original, undispersed soil that is subject to wind erosion. Our baseline approach, hereafter referred to as the Soil Mineral Fraction (SMF) method, assumes that the emitted mineral fractions match the mineral fractions of the wet-sieved soil, which are calculated as follows. Let $f_n^c(\alpha)$ and $f_n^s(\alpha)$ be the soil fraction of mineral n provided by the MMT for the clay and silt-size ranges, respectively, as a function arid soil type α. Then the soil mass fractions of each mineral n at clay and silt sizes relative to the range 0–50 μm, $s_n^c(\alpha,\beta)$ and $s_n^s(\alpha,\beta)$, respectively, are

$$s_n^c(\alpha,\beta) = s^c(\beta) f_n^c(\alpha) \qquad \text{for } n = 1,\ldots,8 \tag{1}$$

$$s_n^s(\alpha,\beta) = s^s(\beta) f_n^s(\alpha) \qquad \text{for } n = 1,\ldots,8 \tag{2}$$

where $s^c(\beta)$ and $s^s(\beta)$ are the soil fractions of clay and silt-sized particles within the range 0–50 μm, respectively, as a function of the soil texture class β (so that $s^c(\beta) + s^s(\beta) = 1$). The MMT prescribes illite, kaolinite, and smectite at clay sizes only ($f_n^c \neq 0$ and $f_n^s = 0$). Feldspar and gypsum are present only at silt sizes ($f_n^c = 0$ and $f_n^s \neq 0$), and calcite, quartz, and hematite are present both at clay and silt sizes ($f_n^c \neq 0$ and $f_n^s \neq 0$). Hematite is not included in the clay-size range of the original MMT [*Claquin et al*., 1999], but we assume following *Nickovic et al*. [2012] that the relative abundance of hematite in the clay fraction is identical to that in the silt fraction provided by the MMT. The soil type and texture databases are described in the supporting information Text S5.

Our new approach is referred to as the Aerosol Mineral Fraction (AMF) method and builds upon brittle fragmentation theory [*Kok*, 2011] to calculate the emitted size distribution given measurements of the wet-sieved soil. The emitted mass fraction of each mineral n at clay and silt sizes relative to the range 0–50 μm, $a_n^c(\alpha,\beta)$ and $a_n^s(\alpha,\beta)$, are calculated as

$$a_n^c(\alpha,\beta) = a^c f_n^c(\alpha);\ a^c = 0.013 \qquad \text{for } n = 1,\ldots,8 \tag{3}$$

$$a_n^s(\alpha,\beta) = \eta(\alpha,\beta)\left[\gamma_n s^c(\beta) f_n^c(\alpha) + s^s(\beta) f_n^s(\alpha)\right] \qquad \text{for } n = 1,\ldots,8 \tag{4}$$

where $a^c = 0.013$ is the mass fraction of emitted clay-sized aerosols relative to the range 0–50 μm, which we assume to be small and independent of location, based upon measurements [*Kok*, 2011]. The emitted silt mass fraction of each mineral n, a_n^s, combines mass of the silt-sized mineral in the wet-sieved soil $\left[s^s(\beta) f_n^s(\alpha)\right]$ with clay soil mass whose aggregates in the original soil were broken during wet sieving $\left[s^c(\beta) f_n^c(\alpha)\right]$. γ_n is a coefficient of proportionality that controls the magnitude of the reaggregation of soil clay mass into emitted silt-sized aggregates (to undo the effect of wet sieving), and η is a parameter that satisfies $\sum_{n=1}^{8}\left(a_n^c + a_n^s\right) = 1$, given γ_n. We set $\gamma_n = 2$ except for quartz (for which $\gamma_n = 0$), assuming this mineral to be indivisible during wet sieving, as in *Perlwitz et al*. [2015a, 2015b]. Equation (4) extends clay soil minerals into the emitted silt-size range, in agreement with measurements by *Kandler et al*. [2009]. This has the effect of reducing the fractional emission of minerals like quartz, which dominates the silt-size fraction of the wet-sieved soil.

The MMT of *Claquin et al*. [1999] omits feldspar and gypsum at clay sizes, even though these minerals are observed at this size both close to sources [e.g,. *Kandler et al*., 2009] and after long-range transport [e.g., *Leinen et al*., 1994; *Arnold et al*., 1998]. Motivated by these observations, we calculate feldspar and gypsum at both clay and silt sizes, albeit separately from equations (3) and (4), as described in the supporting information Text S6.

Equations (1) and (2) and (3) and (4) provide the emitted fractional abundance at clay sizes (0–2 μm) and silt sizes (2–50 μm) for all minerals (except gypsum and feldspar) for the SMF and the AMF methods, respectively. The dust module within ModelE transports five diameter ranges: 0.1–2, 2–4, 4–8, 8–16, and 16–32 μm. The smallest transport bin of our model coincides with the clay-size range, but it remains to distribute the silt-size mineral fractions over the remaining four transport bins. In the AMF, the emitted silt-size mineral fractions are apportioned into the silt-size bins according to the normalized distribution of the volume fraction calculated for each mineral from measurements at Tinfou, Morocco, during times of high concentration [*Kandler et al*., 2009]. We assume that the normalized size distribution of each mineral is spatially invariant. One consequence of the measurements is the apportionment of quartz toward larger particle sizes, compared to other minerals, which suggests its larger characteristic size in the parent soil along with greater resistance to fragmentation. In contrast, for the baseline SMF, we apportion the silt-size mineral fractions across the transport bins without distinguishing among minerals, according to the normalized distribution of total dust mass derived from measurements at Tinfou [*Kandler et al*., 2009]. Some additional details on the differences between the AMF and SMF are provided in the supporting information Text S7.

2.2.2. Modeling Elemental Composition and Missing Minerals

The chemical formula of each mineral that is used to calculate the dust elemental composition from the modeled mineral composition is available in the supporting information Table S1. The use of regionally invariant elemental compositions for each mineral is not only a convenient simplification but also a source of uncertainty in model evaluation. In nature, minerals exhibit regional chemical variations with different ions substituting in the crystal structure [*Shi et al*., 2011; *Journet*, 2008; *Shi et al*., 2012].

Another uncertainty when calculating the model's elemental composition is the lack of certain minerals that could be locally important at the observing site. The MMT provides estimates for eight minerals. *Journet et al*. [2014] provide an expanded mineral database for wet-sieved soils, including estimates for three additional Fe-bearing minerals: vermiculite, chlorite, and goethite. While the use of this database is beyond the scope of our study, in our comparison we will augment the MMT to account for the average abundances of vermiculite and chlorite provided in *Journet et al*. [2014]. Vermiculite is restricted to the clay fraction of the wet-sieved soil and represents ~6% of this fraction. Chlorite is present both in the clay and silt fractions of the soil and represents ~5% and ~6%, respectively. For goethite, instead of using the soil estimates provided in *Journet et al*. [2014], we use estimates specific to dust aerosols arriving at the Canary Islands, where *Lazaro et al*. [2008] measured the average fraction of Fe in hematite relative to Fe in hematite and goethite together: 0.47, which is close to the upper range observed for western Africa (0.22–0.48) [*Formenti et al*., 2014]. We use this relationship to derive the fraction of goethite from the fraction of hematite. In both experiments, we proportionally reduce all other minerals (except hematite) in each size category. In the case of the AMF, we aggregate the additional minerals in the clay fraction of the soil into silt sizes to account for their disintegration by wet sieving. The percent abundances of major elements for these three minerals are provided in the supporting information Table S1.

3. Results and Discussion

3.1. Emitted Mass and Elemental Composition

Figure 1 (top left) displays the percentage of global emission contributed by each size bin for the SMF and the AMF, along with the percent abundances of Si, Al, Fe, Mg, and Ca. The box plots reflect the distribution of this percentage over all combinations of soil texture and soil type. The percent contribution corresponding to each combination is weighted by the total dust emission to emphasize prolific sources. (These values neglect the effect of the three additional iron-bearing minerals, whose effect is considered below).

The large emission of clay-sized particles in the SMF illustrates the effect of wet sieving. Soil aggregates are broken during analysis, creating unrealistically large clay-sized emission in the SMF. This contrasts with the reduced clay-sized emission and relatively uniform size distributions in the AMF that are consistent with theory and observations [*Kok*, 2011; *Perlwitz et al*., 2015b]. The two experiments exhibit similar elemental percentages at clay sizes, but significant contrasts at silt sizes. The median elemental composition of clay-sized emission for both experiments is 23% for Si, 11% for Al, 3% for Fe, 0.6% for Mg, and 3% for Ca. Figure 1 distinguishes Fe from hematite that we refer to as "free Fe," and Fe from other minerals that we refer to as "structural Fe." Most Fe is structural Fe contained in phyllosilicates with the median at clay sizes for each

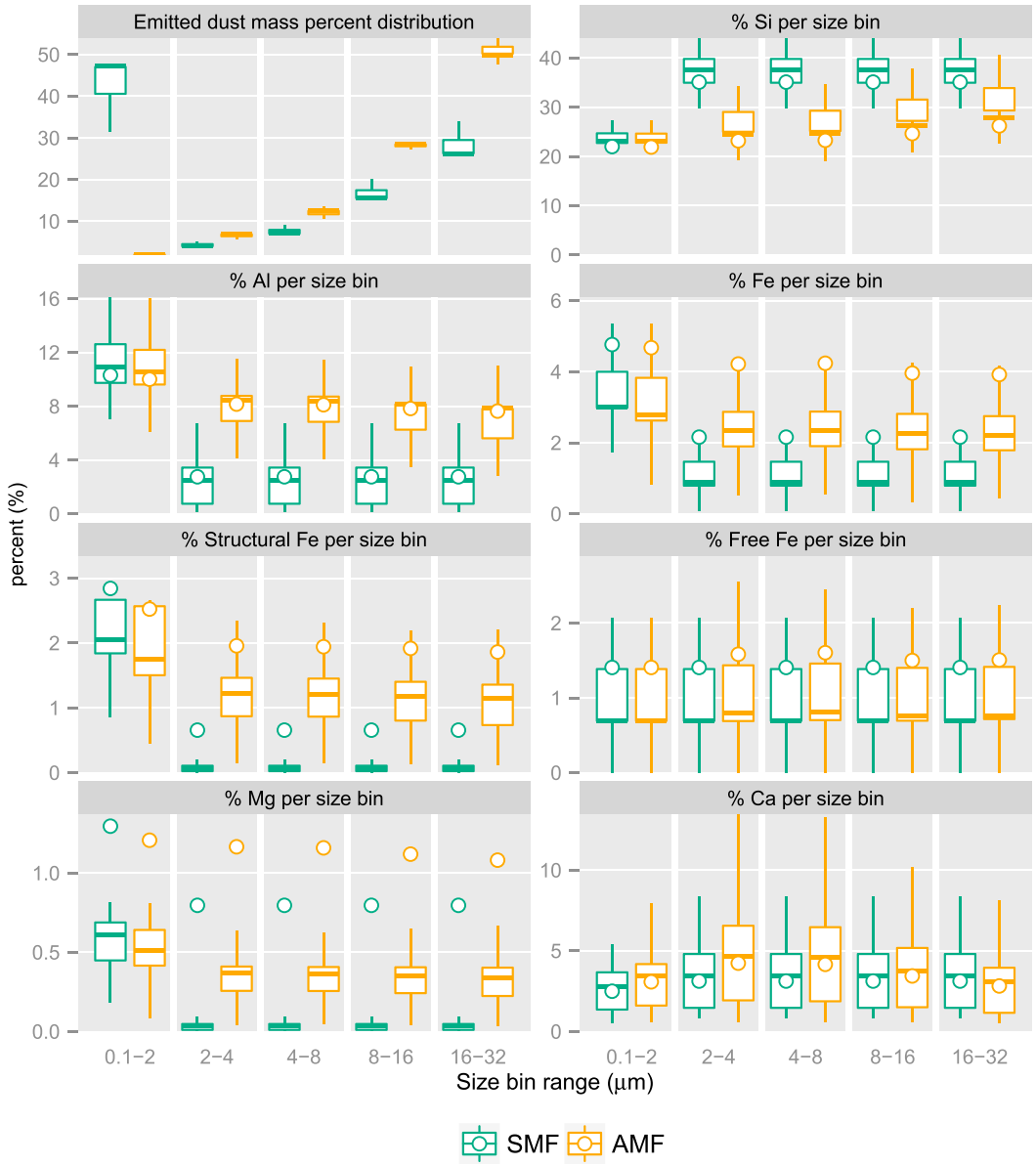

Figure 1. Percent contribution of each size bin to global emission for the SMF (green) and AMF (yellow) experiments. (top left) Total dust mass and (remainder) percent abundance of Si, Al, Fe, structural Fe, free Fe, Mg, and Ca. For each bin, the plot depicts the distribution formed from the 336 combinations of the 12 soil texture categories and the 28 arid soil types included in the MMT. Each combination is weighted by its size-integrated dust emission to emphasize major source regions. The box borders show the first and third quartiles, and the crossbar shows the median. Vertical lines denote minimum and maximum values not exceeding the quartile values by more than a factor of 1.5 times the interquartile distance. Circles represent median values when including the estimated contribution of Fe-bearing minerals vermiculite, chlorite, and goethite.

experiment near 2%, and the rest is free Fe with medians of about 0.6%. The median contribution of each mineral to each element is illustrated in the supporting information Figure S6. At clay sizes, Si is mainly contributed by the phyllosilicates illite and smectite, and to a lesser extent by kaolinite and quartz. The Al abundance is dominated by contributions from kaolinite and illite and to a lesser extent from smectite. Illite and smectite are the largest contributors to structural Fe. Figure 1 shows a slight reduction of structural Fe and Mg at clay sizes in the AMF compared to the SMF, due to our introduction of feldspar and gypsum to the MMT at this size at the expense of phyllosilicates.

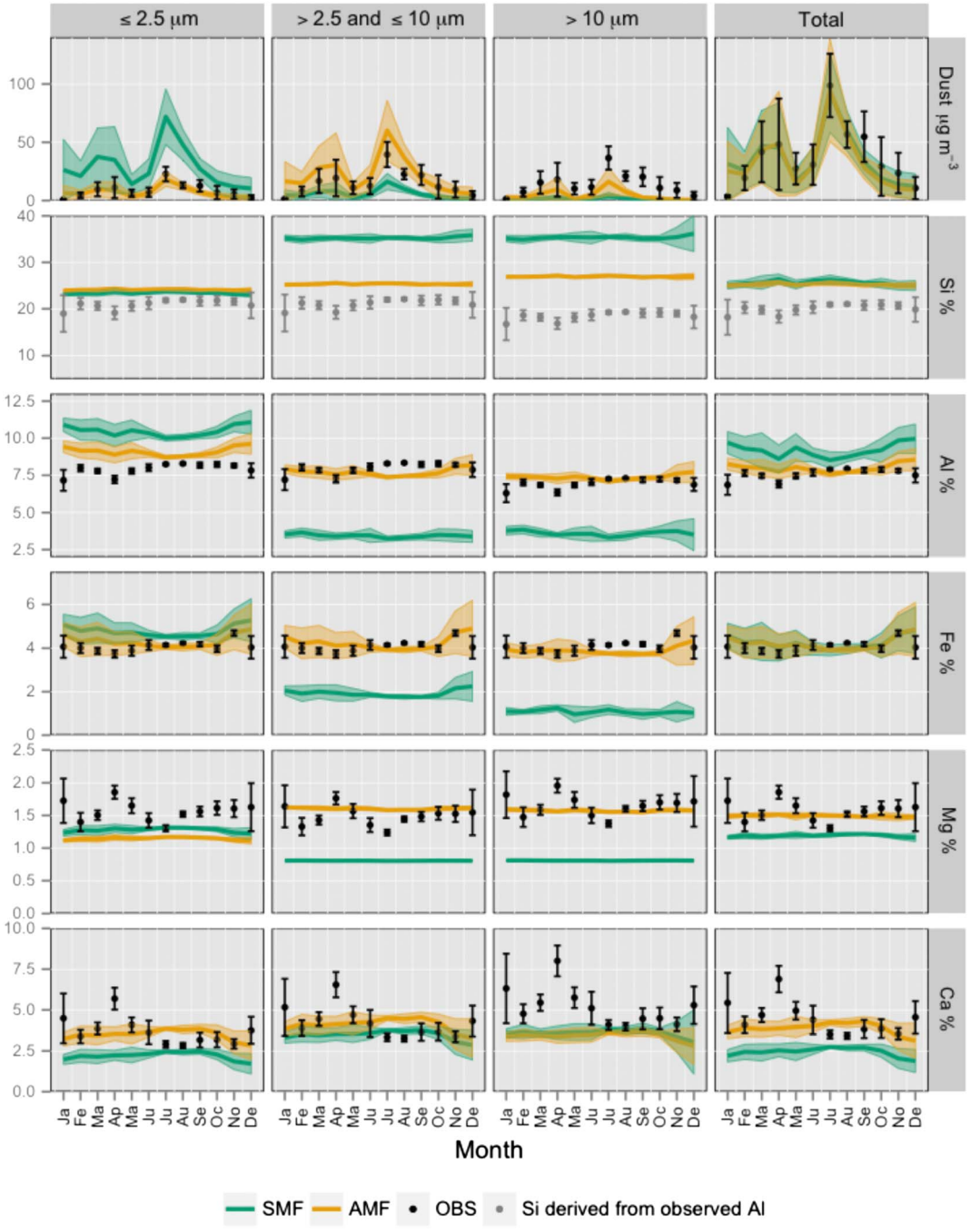

Figure 2. Comparison of the simulated annual cycle with measurements of dust concentration and percent abundances of Si, Al, Fe, Mg, and Ca in fine, coarse, supercoarse, and total dust at Izaña between 2002 and 2010. Green and yellow lines and shading represent the monthly mean and twice the interannual monthly standard deviation for the SMF and AMF experiments, respectively. Measurements are denoted by black dots, whose bar represents twice the intramonthly standard error of each monthly mean. The Si percent abundances are estimated from the measured Al abundances and are displayed in grey. The model results include an estimated contribution of Fe-bearing minerals vermiculite, chlorite, and goethite.

At silt sizes, the Al, structural Fe, and Mg percent abundances are significantly larger, and the Si abundances smaller, in the AMF compared to the SMF. The median Al is augmented from 2 to 8%, structural Fe from 0.08% to 1.2%, and Si is reduced from 37% to ~25%. This clearly illustrates the effect of the restoration of clay-sized Fe and Al-bearing soil particles, created by wet sieving, into emitted silt aggregates in the AMF at the expense of the quartz (the largest contributor of Si at silt sizes in the SMF) and feldspar.

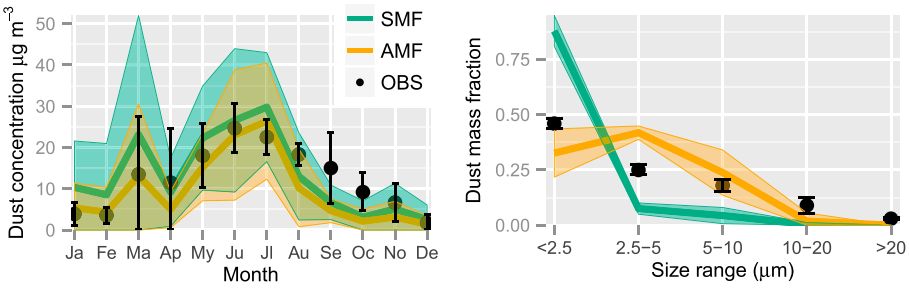

Figure 3. (left) Comparison of the simulated and measured annual cycle of total dust concentration at Barbados between 2002 and 2010. Green and yellow lines and shading represent the monthly means and 2 times the interannual monthly standard deviation for the SMF and AMF experiment, respectively. Measurements are denoted as black dots whose bar represents 2 times the interannual standard deviation. (right) Size distribution of dust mass fraction simulated at Barbados for the SMF (green) and AMF (yellow). The black dot and bar show the monthly mean and one standard deviation of the day-to-day variations, respectively, as observed between 5 April and 3 May 1994.

The circles in Figure 1 are the estimated median percentages after adding the contribution of vermiculite, chlorite, and goethite as described above. Both Fe and Mg are significantly increased both at clay and silt sizes. The median percent contribution of each mineral to each element with this addition is illustrated in the supporting information Figure S7. The increase in Fe comes from structural Fe contributed by vermiculite and chlorite and from increases in free Fe, which approximately doubles with the inclusion of goethite. The median Fe increases from 3% to about 4–5% at clay sizes in both experiments. At silt sizes, the median Fe is approximately doubled in both experiments reaching 2.1% in the SMF and 4.2% in the AMF.

3.2. Dust Concentration and Elemental Composition at Izaña

Figure 2 evaluates the model at Izaña during the period 2002–2010, displaying the measured and simulated annual cycles of monthly concentration of fine, coarse, supercoarse, and total dust. It also displays the annual cycle of the percent abundance of Si, Al, Fe, Mg, and Ca at each size. The estimated contributions of vermiculite, chlorite, and goethite are included, as described above. The comparison neglecting these minerals is available in the supporting information Figure S8.

To compare the AMF and SMF size distributions, we rescaled their concentration at Izaña to match the observed total dust concentration. The model reproduces the observed bimodal annual cycle at Izaña with peaks in March–April and July (Figure 2). The differences between the SMF and AMF are clearly visible in the size dependence of concentration. The SMF roughly triples the observed fine dust concentration and strongly underestimates the concentration of coarse and supercoarse dust. These discrepancies are largely corrected in the AMF, whose fine dust concentration is consistent with observations. The coarse and supercoarse dust concentrations are also closer to the measurements, with slight overestimates and underestimates, respectively.

The discrepancy in the coarse and supercoarse ranges is consistent with the model behavior at other locations [*Perlwitz et al.*, 2015a, 2015b]. The AMF apportions the emitted silt mass within the transport bins using normalized measurements of concentration that are assumed to approximate the size distribution at emission. However, the emitted size distribution is modified by deposition, which preferentially removes the largest particles prior to measurement. Apportionment based upon concentration results in an underestimate of emission at the largest sizes and (because of normalization) a compensating overestimate at the smallest silt sizes.

Measurements at Barbados support our interpretations derived from observations at Izaña (Figure 3, left). Both methods approximately reproduce the annual cycle, including the maximum in early summer, with a secondary peak in March, although they underestimate the total dust in September and October. However, the SMF shows higher total dust throughout the year, particularly between January and March, when it overestimates the observed monthly values by a factor of 2. The overestimation of the Barbados concentration by the SMF is consistent with its unrealistically large fine-mode fraction at Izaña and Barbados (Figure 3, right), which entails a longer dust lifetime.

At Izaña, the observed elemental composition of total dust is 19–21% Si, 7–8% Al, 4% Fe, 1.5–2% Mg, and 3.5–7% Ca (Figure 2). A remarkable feature is the relatively small dependence of the observed Fe, Al, and Mg percentages upon size. For example, Al only slightly decreases from 7–8% in fine and coarse dust to 6–7% in supercoarse dust, and total Fe remains around 4% at all sizes. By restoring Fe and Al-bearing phyllosilicates toward silt sizes, the AMF captures the relatively invariant percentage of Al and Fe at all sizes. Contrarily, the SMF shows an unrealistic decrease of Al and Fe abundances at larger sizes.

For Fe and Al, both experiments show agreement with the observations when the abundances are summed over the entire size range. In the SMF, this agreement is due to the overestimated concentration of fine-mode phyllosilicates compensating for the absence of these minerals in the coarse and supercoarse ranges.

For Si, the SMF overestimates by twofold the observed abundance in coarse and supercoarse sizes. In contrast, the AMF shows reduced abundance closer to the observed value, due to fractional reduction of quartz from the restoration of phyllosilicates at silt sizes. In contrast to other elements, Si is outlined in grey as it is only determined indirectly from the Al content, assuming a constant ratio independent of particle size, and therefore is a more equivocal test of the model.

Certain elemental abundances like Ca and Mg show pronounced seasonal dependence, with maximum values in spring that are not captured by either model. This points toward model underestimation of carbonates and the lack of other evaporate minerals from source regions that affect Izaña in spring. The underestimation of carbonates may be due to the low horizontal resolution of our model or limitations of the MMT that is designed to provide global mean mineral fractions for each soil type that disregard potential regional variations. The underestimation of carbonates was also observed in a global compilation of mineral fractions [*Perlwitz et al*., 2015b].

4. Conclusions

The mineral composition of dust aerosols and the mineral size distributions are key to radiative forcing, ice nucleation, and nutrient deposition to ocean waters. Atlases of soil mineral composition are based upon measurements performed after wet sieving, a process that breaks the aggregates that are found in the undisturbed parent soil that is subject to wind erosion. Our AMF method reconstructs the emitted mineral aggregates destroyed by wet sieving, based upon brittle fragmentation theory and observed size distributions of minerals at silt sizes. We show that by restoring silt-sized aggregates including phyllosilicate soil particles, the AMF method better reproduces the size-resolved dust concentration at Izaña, while explaining the relatively invariant percent abundance of Fe and Al across size ranges. Our attribution of the improvement of Fe abundance to this restoration is possible, because our model distinguishes between structural Fe in clays (that we restore at silt sizes) and free Fe found in iron oxides. In contrast, the SMF method reproduces only the total (size-integrated) concentration, and only because of compensation of the underestimated silt mass by an excessive abundance of clay-sized particles. This spurious agreement shows the value of size-resolved measurements of mineral and elemental composition. The detailed observational record at Izaña supports the conclusions of recent papers [*Perlwitz et al*., 2015a, 2015b], whose evaluation was limited to sporadic measurements of mineral fractions. In general, measurements of elemental composition are abundant compared to those of mineral fractions; the former is an underutilized source of model evaluation. A remaining challenge is to characterize regional variations of chemical composition for dust minerals.

Acknowledgments

Data from the Izaña Observatory and Barbados can be obtained by request to Sergio Rodríguez and Joseph M. Prospero, respectively. The dust mineral fractions at emission for the SMF and AMF methods can be downloaded from http://data.giss.nasa.gov/mineralfrac/. This research was supported by the Department of Energy (DE-SC0006713), the NASA Modeling, Analysis and Prediction Program, and the Aerosol Global Atmospheric Watch program of Izaña Observatory, which has been funded by AEMET and several research projects of the Ministry of Economy and Competitiveness of Spain and the European Regional Development Fund (ERDF) including POLLINDUST (CGL2011-26259) and AEROATLAN (CGL2015-66229-P). Chemical analysis was made at IDAEA-CSIC (A. Alastuey and X. Querol). Computational resources were provided by the NASA High-End Computing (HEC) Program through the NASA Center for Climate Simulation (NCCS) at Goddard Space Flight Center.

References

Alonso-Pérez, S., E. Cuevas, C. Pérez, X. Querol, J. M. Baldasano, R. Draxler, and J. J. de Bustos (2011), Trend changes of African airmass intrusions in the marine boundary layer over the subtropical eastern North Atlantic region in winter, *Tellus B*, *63*, 255–265.

Alonso-Pérez, S., E. Cuevas, X. Querol, J. C. Guerra, and C. Pérez (2012), African dust source regions for observed dust outbreaks over the Subtropical Eastern North Atlantic region, above 25°N, *J. Arid Environ.*, *78*, 100–109.

Arnold, E., J. Merrill, M. Leinen, and J. King (1998), The effect of source area and atmospheric transport on mineral aerosol collected over the North Pacific Ocean, *Global Planet. Change*, *18*, 137–159, doi:10.1016/S0921-8181(98)00013-7.

Bauer, S. E., and D. Koch (2005), Impact of heterogeneous sulfate formation at mineral dust surfaces on aerosol loads and radiative forcing in the Goddard Institute for Space Studies general circulation model, *J. Geophys. Res.*, *110*, D17202, doi:10.1029/2005JD005870.

Chen, H., J. G. Navea, M. A. Young, and V. H. Grassian (2011), Heterogeneous photochemistry of trace atmospheric gases with components of mineral dust aerosol, *J. Phys. Chem. A*, *115*, 490–499, doi:10.1021/jp110164j.

Claquin, T., M. Schulz, and Y. J. Balkanski (1999), Modeling the mineralogy of atmospheric dust sources, *J. Geophys. Res.*, *104*, 22,243–22,256, doi:10.1029/1999JD900416.

DeMott, P. J., K. Sassen, M. R. Poellot, D. Baumgardner, D. C. Rogers, S. D. Brooks, A. J. Prenni, and S. M. Kreidenweis (2003), African dust aerosols as atmospheric ice nuclei, *Geophys. Res. Lett.*, *30*(14), 1732, doi:10.1029/2003GL017410.

Formenti, P., S. Caquineau, S. Chevaillier, A. Klaver, K. Desboeufs, J. L. Rajot, S. Belin, and V. Briois (2014), Dominance of goethite over hematite in iron oxides of mineral dust from Western Africa: Quantitative partitioning by X-ray absorption spectroscopy, *J. Geophys. Res. Atmos.*, *119*, 12,740–12,754, doi:10.1002/2014JD021668.

Jickells, T. D., et al. (2005), Global iron connections between desert Dust, ocean biogeochemistry, and climate, *Science*, *308*, 67–71, doi:10.1126/science.1105959.

Journet, E. (2008), Study of mineralogical factor on iron dust solubility and on iron redox state in the biogeochemical context of iron inputs to surface ocean, PhD thesis, 257 pp., Université Paris-Diderot - Paris VII. [Available at https://tel.archives-ouvertes.fr/tel-00555491.]

Journet, E., Y. Balkanski, and S. P. Harrison (2014), A new data set of soil mineralogy for dust-cycle modeling, *Atmos. Chem. Phys.*, *14*, 3801–3816, doi:10.5194/acp-14-3801-2014.

Kandler, K., et al. (2009), Size distribution, mass concentration, chemical and mineralogical composition and derived optical parameters of the boundary layer aerosol at Tinfou, Morocco, during SAMUM 2006, *Tellus B*, *61*, 32–50, doi:10.1111/j.1600-0889.2008.00385.x.

Knippertz, P., and M. C. Todd (2012), Mineral dust aerosols over the Sahara: Meteorological controls on emission and transport and implications for modeling, *Rev. Geophys.*, *50*, RG1007, doi:10.1029/2011RG000362.

Kok, J. F. (2011), A scaling theory for the size distribution of emitted dust aerosols suggests climate models underestimate the size of the global dust cycle, *Proc. Natl. Acad. Sci. U.S.A.*, *108*, 1016–1021, doi:10.1073/pnas.1014798108.

Lazaro, F. J., L. Gutiérrez, V. Barrón, and M. D. Gelado (2008), The speciation of iron in desert dust collected in Gran Canaria (Canary Islands): Combined chemical, magnetic and optical analysis, *Atmos. Environ.*, *42*(40), 8987–8996.

Leinen, M., J. M. Prospero, E. Arnold, and M. Blank (1994), Mineralogy of aeolian dust reaching the North Pacific Ocean 1. Sampling and analysis, *J. Geophys. Res.*, *99*, 21,017–21,023, doi:10.1029/94JD01735.

Li-Jones, X., and J. M. Prospero (1998), Variations in the size distribution of non-sea-salt sulfate aerosol in the marine boundary layer at Barbados: Impact of African dust, *J. Geophys. Res.*, *103*(D13), 16,073–16,084, doi:10.1029/98JD00883.

Miller, R. L., et al. (2006), Mineral dust aerosols in the NASA Goddard Institute for Space Sciences ModelE atmospheric general circulation model, *J. Geophys. Res.*, *111*, D06208, doi:10.1029/2005JD005796.

Miller, R. L., P. Knippertz, C. Pérez García-Pando, J. P. Perlwitz, and I. Tegen (2014a), Impact of dust radiative forcing upon climate, in *Mineral Dust: A Key Player in the Earth System*, edited by P. Knippertz and J.-B. W. Stuut, pp. 327-357, Springer, Dordrecht, Netherlands, doi:10.1007/978-94-017-8978-3_13.

Miller, R. L., et al. (2014b), CMIP5 historical simulations (1850–2012) with GISS ModelE2, *J. Adv. Model. Earth Syst.*, *6*(2), 441–477, doi:10.1002/2013MS000266.

Nickovic, S., A. Vukovic, M. Vujadinovic, V. Djurdjevic, and G. Pejanovic (2012), Technical Note: High-resolution mineralogical database of dust-productive soils for atmospheric dust modeling, *Atmos. Chem. Phys.*, *12*, 845–855, doi:10.5194/acp-12-845-2012.

Pérez, C., S. Nickovic, G. Pejanovic, J. M. Baldasano, and E. Özsoy (2006), Interactive dust-radiation modeling: A step to improve weather forecast, *J. Geophys. Res.*, *111*, D16206, doi:10.1029/2005JD006717.

Pérez García-Pando, C., et al. (2014), Soil dust aerosols and wind as predictors of seasonal meningitis incidence in Niger, *Environ. Health Perspect.*, *122*, 679–686, doi:10.1289/ehp.1306640.

Perlwitz, J. P., C. Pérez García-Pando, and R. L. Miller (2015a), Predicting the mineral composition of dust aerosols—Part 1: Representing key processes, *Atmos. Chem. Phys.*, *15*, 11,593–11,627, doi:10.5194/acp-15-11593-2015.

Perlwitz, J. P., C. Pérez García-Pando, and R. L. Miller (2015b), Predicting the mineral composition of dust aerosols—Part 2: Model evaluation and identification of key processes with observations, *Atmos. Chem. Phys.*, *15*, 11,629–11,652, doi:10.5194/acp-15-11629-2015.

Prospero, J. M. (1999), Long-term measurements of the transport of African mineral dust to the southeastern United States: Implications for regional air quality, *J. Geophys. Res.*, *104*(D13), 15,917–15,927, doi:10.1029/1999JD900072.

Prospero, J. M., and T. N. Carlson (1972), Vertical and areal distribution of Saharan dust over the western Equatorial North Atlantic Ocean, *J. Geophys. Res.*, *77*, 5255–5265, doi:10.1029/JC077i027p05255.

Prospero, J. M., and P. J. Lamb (2003), African droughts and dust transport to the Caribbean: Climate change implications, *Science*, *302*(5647), 1024–1027.

Prospero, J. M., and O. L. Mayol-Bracero (2013), Understanding the transport and impact of African dust on the Caribbean Basin, *Bull. Am. Meteorol. Soc.*, *94*(9), 1329–1337, doi:10.1175/BAMS-D-12-00142.1.

Querol, X., A. Alastuey, S. Rodríguez, F. Plana, E. Mantilla, and C. R. Ruiz (2001), Monitoring of PM10 and PM2.5 around primary particulate anthropogenic emission sources, *Atmos. Environ.*, *35*, 845–858.

Rayner, N. A., D. E. Parker, E. B. Horton, C. K. Folland, L. V. Alexander, D. P. Rowell, E. C. Kent, and A. Kaplan (2003), Global analyses of sea surface temperature, sea ice, and night marine air temperature since the late nineteenth century, *J. Geophys. Res.*, *108*(D14), 4407, doi:10.1029/2002JD002670

Rodríguez, S., A. Alastuey, S. Alonso-Pérez, X. Querol, E. Cuevas, J. Abreu-Afonso, M. Viana, N. Pérez, M. Pandolfi, and J. de la Rosa (2011), Transport of desert dust mixed with North African industrial pollutants in the subtropical Saharan Air Layer, *Atmos. Chem. Phys.*, *11*, 6663–6685, doi:10.5194/acp-11-6663-2011.

Rodríguez, S., A. Alastuey, and X. Querol (2012), A review of methods for long term in situ characterization of aerosol dust, *Aeolian Res.*, *6*, 55–74, doi:10.1016/j.aeolia.2012.07.004.

Rodríguez, S., E. Cuevas, J. M. Prospero, A. Alastuey, X. Querol, J. López-Solano, M. I. García, and S. Alonso-Pérez (2015), Modulation of Saharan dust export by the North African dipole, *Atmos. Chem. Phys.*, *15*, 7471–7486, doi:10.5194/acp-15-7471-2015.

Schmidt, G. A., et al. (2014), Configuration and assessment of the GISS ModelE2 contributions to the CMIP5 archive, *J. Adv. Model. Earth Sys.*, *6*, 141–184, doi:10.1002/2013MS000265.

Seifert, P., A. Ansmann, I. Mattis, U. Wandinger, M. Tesche, R. Engelmann, D. Müller, C. Pérez, and K. Haustein (2010), Saharan dust and heterogeneous ice formation: Eleven years of cloud observations at a central European EARLINET site, *J. Geophys. Res.*, *115*, D20201, doi:10.1029/2009JD013222.

Shao, Y. (2001), A model for mineral dust emission, *J. Geophys. Res.*, *106*, 20,239–20,254, doi:10.1029/2001JD900171.

Shi, Z., et al. (2011), Influence of chemical weathering and aging of iron oxides on the potential iron solubility of Saharan dust during simulated atmospheric processing. *Global Biogeochem. Cycles*, *25*, GB2010, doi:10.1029/2010GB003837.

Shi, Z., M. D. Krom, T. D. Jickells, S. Bonneville, K. S. Carslaw, N. Mihalopoulos, A. R. Baker, and L. G. Benning (2012), Impacts on iron solubility in the mineral dust by processes in the source region and the atmosphere: A review, *Aeolian Res.*, *5*(21–42), 1875–9637, doi:10.1016/j.aeolia.2012.03.001.

Slingo, A., et al. (2006), Observations of the impact of a major Saharan dust storm on the atmospheric radiation balance, *Geophys. Res. Lett.*, *33*, L24817, doi:10.1029/2006GL027869.

Tsamalis, C., A. Chédin, J. Pelon, and V. Capelle (2013), The seasonal vertical distribution of the Saharan Air Layer and its modulation by the wind, *Atmos. Chem. Phys.*, *13*, 11,235–11,257, doi:10.5194/acp-13-11235-2013.